LETTERS

Hydrous olivine unable to account for conductivity anomaly at the top of the asthenosphere

Takashi Yoshino[1], Takuya Matsuzaki[1], Shigeru Yamashita[1] & Tomoo Katsura[1]

The oceanic asthenosphere is observed to have high electrical conductivity, which is highly anisotropic in some locations[1,2]. In the directions parallel and normal to the plate motion, the conductivity is of the order of 10^{-1} and 10^{-2} S m^{-1}, respectively, which cannot be explained by the conductivity of anhydrous olivine[2]. But because hydrogen can be incorporated in olivine at mantle pressures[3–5], this observation has been attributed to olivine hydration, which might cause anisotropically high conductivity by proton migration[1,2,6,7]. To examine this hypothesis, here we report the effect of water on electrical conductivity and its anisotropy for hydrogen-doped and undoped olivine at 500–1,500 K and 3 GPa. The hydrous olivine has much higher conductivity and lower activation energy than anhydrous olivine in the investigated temperature range. Nevertheless, extrapolation of the experimental results suggests that conductivity of hydrous olivine at the top of the asthenosphere should be nearly isotropic and only of the order of 10^{-2} S m^{-1}. Our data indicate that the hydration of olivine cannot account for the geophysical observations[2], which instead may be explained by the presence of partial melt elongated in the direction of plate motion.

The electrical conductivity of hydrogen-bearing nominally anhydrous minerals has not been previously determined owing to the difficulty of reliable measurement; hydrogen inside silicate minerals can easily escape under high temperature conditions (above 1,000 K) because of its high diffusivity. Recently, electrical conductivity of hydrous wadsleyite and ringwoodite has been reported, based on measurements over quite short times at a single temperature condition for each run in order to minimize water loss[8]. However, this method cannot determine a reliable activation energy because of the absence of systematic measurements over a wide temperature range. There are two approaches to overcoming the above problem: one is to measure conductivity in a closed system for H_2O, and the other is to measure conductivity at low temperatures at which the hydrogen diffusion rate is sufficiently low. The former is impractical, because of the difficulty of sealing-in H_2O by using an insulating material. Although electrical conductivity measurements under low temperature conditions (<1,000 K) require high insulation resistance, we have measured the electrical conductivity of hydrous olivine at temperatures of 500–1,000 K using low frequency (0.01 Hz) a.c. signals. To clarify the effect of hydrogen on the electrical conductivity, we have conducted conductivity measurements both for initially hydrogen-doped samples and for undoped samples.

The conductivity measurements were conducted at 3 GPa in a Kawai-type multi-anvil apparatus along several heating–cooling cycles in each run (see Supplementary Methods). Figure 1 is an Arrhenius plot showing conductivities of the hydrogen-doped and the undoped olivines along the three principal axes. The hydrogen-doped olivine has a higher conductivity (by two orders of magnitude) than the undoped olivine. The conductivity of the hydrogen-doped olivine is anisotropic in the investigated temperature range; it is higher along the [100] crystallographic axis than the [010] and [001] axes when data are normalized to the same hydrogen content, based on a linear relationship between the hydrogen concentration and the conductivity. The trend of anisotropy is consistent with that of hydrogen diffusion in olivine[7]. The conductivity of the undoped olivine can be divided into two regions. At lower temperatures, the conductivity has a smaller temperature dependence than it has at higher temperatures. In each temperature region, the logarithmic conductivity increases linearly with decreasing reciprocal temperature. The conductivity in the high temperature region is consistent with that of anhydrous olivine previously obtained[9].

Electrical conductivities σ can be expressed as follows:

$$\sigma = \sigma_0 \exp\left(-\frac{E}{kT}\right) \quad (1)$$

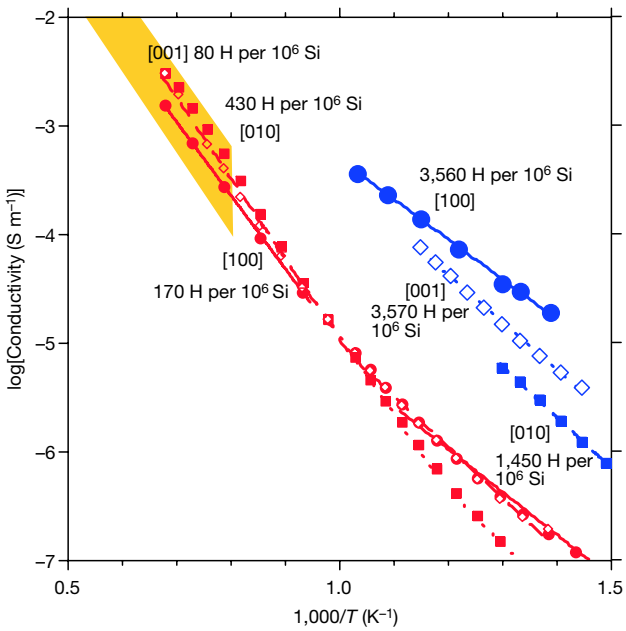

Figure 1 | Electrical conductivity of olivine as a function of reciprocal temperature. The symbols indicate raw data for each sample with different hydrogen contents. Red and blue lines indicate results for the undoped and the hydrogen-doped samples, respectively. Filled circles, filled squares and open diamonds represent the different crystallographic directions: [100], [010] and [001], respectively. Solid, dotted and dashed lines indicate the data fitting for [100], [010] and [001] directions, respectively. The yellow area indicates the range of conductivity of anhydrous olivine at 4 GPa reported previously[9].

[1]Institute for Study of the Earth's Interior, Okayama University, Misasa, Tottori 682-0193, Japan.

Table 1 | Summary of experimental runs

Run no.	Axis	C_{OH}*	C_{OH}†	σ_{0h}‡	E_h‡ (eV)	σ_{0P}§	E_P§ (eV)	Remarks
1K520	[100]	0(20)	168(58)	65.04	1.35	0.055	0.78	
1K524	[010]	0(12)	433(156)	169.9	1.42	0.384	0.98	
1K521	[001]	0(7)	82(47)	286.2	1.47	0.250	0.89	
1K471	[100]	3,560(187)	3,503(189)			2.329	0.73	
1K482	[010]	1,450(291)	700(224)			7.416	0.93	Dehydration
1K478	[001]	3,569(128)	1,118(124)			7.666	0.87	Dehydration

All experiments were conducted at 3 GPa.
* Hydrogen concentration (in H per 10^6 Si) of synthesized hydrous olivine before the conductivity measurement experiment, determined by FTIR spectroscopy. Parentheses denote one standard deviation for five analyses.
† Hydrogen concentration (in H per 10^6 Si) after the conductivity measurement experiment.
‡ Pre-exponential factor (σ_{0h}) and activation energy (E_h) for hopping conductivity in the higher temperature range.
§ Pre-exponential factor (σ_{0P}) and activation energy (E_P) for proton conductivity of hydrous olivine. For the relatively dry olivine, they were calculated in the lower temperature range.

where σ_0 is a pre-exponential factor, E is activation energy, k is the Boltzmann constant and T is temperature. The pre-exponential term and activation energy are summarized in Table 1. The activation energies of the undoped olivine in the high temperature region are around 1.4 eV, which is consistent with the previous studies[9–11]. In this temperature region, transport of small polarons should be the dominant conduction mechanism. The activation energies of the hydrogen-doped olivine along each crystallographic axis are found to be $E_{[100]} = 0.73$, $E_{[010]} = 0.97$ and $E_{[001]} = 0.87$ eV. These values are essentially identical to those of the undoped olivine in the lower temperature region: $E_{[100]} = 0.78$, $E_{[010]} = 0.98$ and $E_{[001]} = 0.89$ eV. These observations suggest that the conduction mechanism of the undoped olivine in the lower temperature region should be attributed to migration of hydrogen (proton conduction). In fact, the undoped olivine contained a small amount (80–400 H per 10^6 Si) of hydrogen during the electrical conductivity measurements (Table 1). We suggest that the intrinsic (small polaron) conductivity of olivine is masked by the extrinsic (proton) conductivity, owing to the difference of the activation energy between these two mechanisms. The fact that the activation energy of the proton conduction for the [100] direction is lower than for the other axes suggests that the anisotropy of the proton conductivity becomes small, and [010] rather than [100] becomes the highest conductive direction, at high temperatures.

The activation energies for proton conduction are generally lower than those obtained from proton diffusion experiments[7]. At the temperature range of 1,073–1,273 K, the proton conductivity is nearly isotropic, whereas the proton diffusion in the [100] direction is significantly faster than that in the other directions[7]. These discrepancies may imply that the experimental series of diffusion and conduction measurements are controlled by different migration mechanisms of protons in olivine crystal. The hydrogen concentrations for the conduction experiments were nearly in equilibrium, whereas those for the diffusion experiments were not in equilibrium (for details, see Supplementary Discussion). On the other hand, hydrogen diffusion data for wadsleyite[12] also show that the activation energy for proton diffusion (0.92 eV) is clearly higher than that for proton conduction (0.66 eV)[8]. This tendency is same as for the case of olivine. Therefore, mechanisms of proton migration for these two phenomena could be essentially different. In other words, proton diffusion measurements are not necessarily an appropriate way to estimate proton conductivity.

To assess the presence of water in the upper mantle, we compare the present experimental data with the electromagnetic study underneath the Pacific Ocean; we do this by calculating the logarithmic conductivity of hydrous olivine versus depth, based on the following assumptions (Fig. 2). A potential temperature of 1,623 K was assumed for the adiabatic geotherm. Activation energies for proton conductivity were assumed to be constant at temperatures higher than the present measurement range. The upper limit of the electrical conductivity for hydrous olivine down to a depth of 410 km was calculated on the basis of the reported pressure dependence of the maximum H_2O solubility in olivine[13]. A linear relation between conductivity and amount of hydrogen was assumed, based on the Nernst–Einstein relation[14]. The oxygen fugacity in the mantle was assumed to be the Ni/NiO buffer[15], although that in the sub-ridge mantle is two orders of magnitude less than Ni/NiO (ref. 16).

The electrical conductivity in the oceanic upper mantle above 400 km depth varies from $\sim 10^{-3}$ to 10^{-1} S m^{-1} (refs 1, 2, 17, 18). The one-dimensional electrical conductivity structure in the mantle of the one-fourth of the Earth beneath the north Pacific Ocean obtained by a semi-global electromagnetic induction study[17] is quite consistent with the laboratory-based conductivity–depth profile predicted from the dry olivine[9]. In contrast, the deep electrical conductivity profile, obtained from analysis of data from a submarine cable

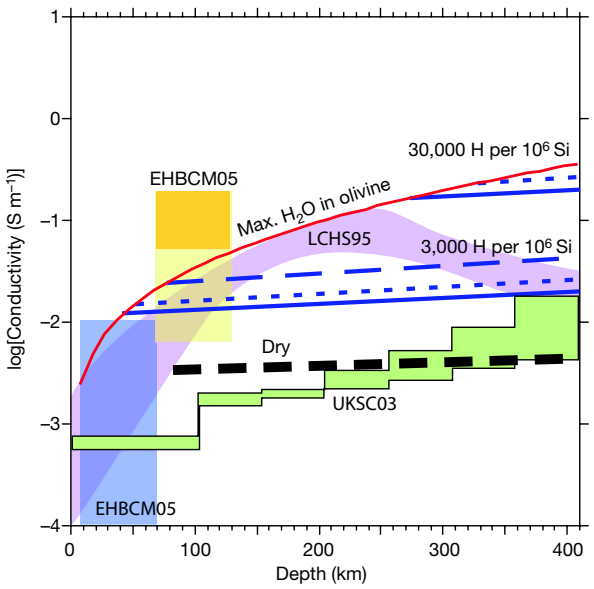

Figure 2 | Comparison of laboratory data on electrical conductivity of hydrous olivine as a function of H_2O content with the geophysically observed electrical conductivity in the upper mantle beneath the Pacific. The red line indicates the upper bound of the electrical conductivity of the hydrous olivine. Because the maximum hydroxyl solubility as a function of depth based on equation (1) of ref. 12 is three times the hydrogen content based on a method of ref. 5, we applied one-third the value of the hydrogen content used by ref. 12 as the hydrogen content of olivine. The blue solid line, long-dashed line and short-dashed line represent the electrical conductivity of hydrous olivine in the [100], [010] and [001] directions, respectively. The electrical conductivity of hydrous olivine for each crystallographic direction is normalized to 3,000 and 30,000 H per 10^6 Si, respectively. XSD00[9] (thick black dashed line) shows the electrical conductivity of dry olivine. The green and pink areas (UKSC03[17] and LCHS95[18]) represent the geophysically observed conductivity profile in the Pacific. The orange and light-orange regions (EHBCM05[2]) indicate the range of conductivity in directions parallel to and normal to the plate motion around a depth of 100 km near the East Pacific Rise. The light blue area (EHBCM05[2]) represents the range of conductivity above 60 km near the East Pacific Rise.

extending from Hawaii to North America, showed a conductivity peak of 10^{-1} S m^{-1} at the depth range 200–250 km (ref. 18). This profile is quite consistent with the upper limit of the conductivity predicted from the maximum H_2O solubility in olivine. Therefore, the high-conductivity anomaly in a part of the mantle underneath the Pacific Ocean can be interpreted as the presence of $\sim 10^4$ H per 10^6 Si, which is less than the storage capacity of H_2O in olivine. The variation in the conductivity–depth profiles may be derived from the local heterogeneity of the H_2O distribution in the mantle.

A recent magnetotelluric study at the southern East Pacific Rise reported two important features of the electrical conductivity profile near a mid-ocean ridge[2]. The conductivity largely increases with increasing depth from 50 to 100 km. It also becomes strongly anisotropic in this depth range. Around 100 km, the difference of conductivities between the direction parallel (10^{-1} S m^{-1}) and normal (10^{-2} S m^{-1}) to the plate motion reaches one order of magnitude. This remarkable change was interpreted as an increase in H_2O content in olivine in this depth range. However, the present results cannot support the hydrous olivine hypothesis. First, the estimated conductivity of hydrous olivine at a depth of 100 km can be only as high as 10^{-2} S m^{-1} in this region. Although this value is distinctly higher than that of dry olivine[9–11], it is not enough to explain the maximum conductivity ($\sim$0.1 S m^{-1}) obtained from the East Pacific Rise. To explain the conductivity of 0.1 S m^{-1}, a hydrogen concentration of over 17,000 H per 10^6 Si, which exceeds the maximum solubility of H_2O in olivine at 3 GPa (ref. 5), is required. Second, extrapolation of our data to high temperatures shows that anisotropy of hydrous olivine becomes small (less than by a factor of 2) at the temperature condition corresponding to the top of the asthenosphere. The weak anisotropy disagrees with the one-order-of-magnitude difference of the conductivity between ridge-parallel and ridge-normal directions.

In addition, seismic observations showed high shear velocity in the direction parallel to plate motion. The seismic anisotropy was interpreted as horizontal alignment of the olivine [100] axis, which has the highest shear wave velocity among the crystallographic axes, in the direction of spreading[19]. The concentration of [100] to the shear direction is consistent with the olivine fabric deformed under the dry condition. However, the present results suggest that the conductivity of olivine is lowest in the [100] direction. Hence, if the hydrous olivine is oriented in the direction of the [100] axis, as suggested by the seismic study, conductivity in the direction of the plate motion should be lowest, which is opposite to the results of the magnetotelluric study. Increase of the H_2O content may change the olivine fabric[20]. Taking the crystallographic direction [010] with the highest conductivity at higher temperature conditions into account, it is unlikely that the olivine fabric could explain the highest conductivity direction, even if plastic deformation occurs under both dry ([100] parallel to the shear direction) and wet ([001] parallel to the shear direction) conditions[20]. These discrepancies lead us to conclude that the geophysically observed high conductivity anomaly[2] cannot be attributed to the conductivity of hydrous olivine.

An alternative explanation for the high conductivity anomaly is that the conductivity is controlled by a presence of partial melt in this region. Basaltic melt itself has higher electrical conductivity ($>10^{-0.5}$ S m^{-1})[21], and the wetting properties of the basaltic melt against olivine allow the interconnection of partial melt[22]. Thus, partial melting of peridotites could cause the high conductivity anomaly[23]. The top of the asthenosphere ($\sim$60 km) is a region where partial melting of dry peridotite occurs beneath a mid-ocean ridge[24]. For a normal geotherm with a potential temperature of 1,623 K, partial melting of peridotite is, however, unlikely to occur at the deeper zone ($\sim$100 km) and at locations far from the ridge. Some factors such as water[25], carbon dioxide[26] and a potassium-rich composition[27] should be considered as lowering the melting temperature. For example, the presence of 400 p.p.m. (by weight) of H_2O in peridotite can cause partial melting[13].

The top of the asthenosphere along the normal geotherm could allow the existence of partial melt, even though the amount of the components lowering the melting temperature is small. If the lithosphere is actually impermeable to the partial melt[2], partial melt could be trapped at the top of the asthenosphere. It is possible that a small amount of melt is successively added to the top of the asthenosphere from the deeper region, because the flow of mantle convection near the ridge axis should have a considerably large horizontal dimension[19,28]. The electromagnetic and seismic data obtained from the region just beneath the ridge axis, showing the presence of a narrow melt conduit[29,30], may support the presence of an impermeable layer at the top of the asthenosphere.

The high anisotropy of conductivity in the direction of plate motion[2] can be explained by anisotropic interconnection of melt in the partial melting hypothesis. A recent electromagnetic observation depicted a high-conductivity zone with high anisotropy in the vertical direction beneath the East Pacific Rise[29]. The origin of this zone is attributed to vertical melt interconnection caused by the material flow. Therefore, we can expect that at the top of the asthenosphere in the region near the ridge, the partial melt should be better connected in the direction of plate motion, which will cause the observed anisotropy of conductivity.

Received 6 December 2005; accepted 22 August 2006.

1. Karato, S. The role of hydrogen in the electrical conductivity of the upper mantle. *Nature* **347**, 272–273 (1990).
2. Evans, R. L. *et al.* Geophysical evidence from the MELT area for compositional controls on oceanic plates. *Nature* **437**, 249–252 (2005).
3. Bai, Q. & Kohlstedt, D. L. Substantial hydrogen solubility in olivine and implications for water storage in the mantle. *Nature* **357**, 672–674 (1992).
4. Bell, D. R. & Rothman, G. R. Water in the earth's mantle: the role of nominally anhydrous minerals. *Science* **255**, 1391–1397 (1992).
5. Kohlstedt, D. L., Keppler, H. & Rubie, D. C. Solubility of water in the α, β and γ phases of $(Mg,Fe)_2SiO_4$. *Contrib. Mineral. Petrol.* **123**, 345–357 (1996).
6. Mackwell, S. J. & Kohlstedt, D. L. Diffusion of hydrogen in olivine: implications for water in mantle. *J. Geophys. Res.* **95**, 5079–5088 (1990).
7. Kohlstedt, D. L. & Mackwell, S. J. Diffusion of hydrogen and intrinsic point defects in olivine. *Z. Phys. Chem.* **207**, 147–162 (1998).
8. Huang, X., Xu, Y. & Karato, S. Water content in the transition zone from electrical conductivity of wadsleyite and ringwoodite. *Nature* **434**, 746–749 (2005).
9. Xu, Y., Shankland, T. J. & Duba, A. G. Pressure effect on electrical conductivity of mantle olivine. *Phys. Earth Planet. Inter.* **118**, 149–161 (2000).
10. Shankland, T. J. & Duba, A. G. Standard electrical conductivity of isotropic, homogeneous olivine in the temperature range 1200°-1500°C. *Geophys. J. Int.* **103**, 25–31 (1990).
11. Wanamaker, B. J. & Duba, A. G. Electrical conductivity of San Carlos olivine along [100] under oxygen- and pyroxene-buffered conditions and implications for defect equilibria. *J. Geophys. Res.* **98**, 489–500 (1993).
12. Hae, R., Ohtani, E., Kubo, T., Koyama, T. & Utada, H. Hydrogen diffusivity in wadsleyite and water distribution in the mantle transition zone. *Earth Planet. Sci. Lett.* **243**, 141–148 (2006).
13. Hirschmann, M. M., Aubaud, C. & Withers, A. C. Storage capacity of H_2O in nominally anhydrous minerals in the upper mantle. *Earth Planet. Sci. Lett.* **236**, 167–181 (2005).
14. Mott, N. F. & Gurney, R. W. *Electronic Processes in Ionic Crystals* (Oxford Univ. Press, Oxford, 1948).
15. Wood, B. J., Btyndzia, L. T. & Johnson, K. E. Mantle oxidation state and its relationship to tectonic environment and fluid speciation. *Science* **248**, 337–345 (1990).
16. Williams, H. M. *et al.* Iron isotope fractionation and the oxygen fugacity of the mantle. *Science* **304**, 1656–1659 (2004).
17. Utada, H., Koyama, T., Shimizu, H. & Chave, A. D. A semi-global reference model for electrical conductivity in the mid-mantle beneath the north Pacific region. *Geophys. Res. Lett.* **30**, 1194, doi:10.1029/2002GL016902 (2003).
18. Lizzarralde, D., Chave, A. D., Hirth, G. & Schultz, A. Northeastern Pacific mantle conductivity profile from long-period magnetotelluric sounding using Hawaii to California submarine cable data. *J. Geophys. Res.* **100**, 17837–17854 (1995).
19. The MELT seismic team. Imaging the deep seismic structure beneath a mid-ocean ridge: The MELT experiment. *Science* **280**, 1215–1218 (1998).
20. Jung, H. & Karato, S. Water-induced fabric transitions in olivine. *Science* **293**, 1460–1463 (2001).
21. Presnall, D. C., Simmons, C. L. & Porath, H. Change of electrical conductivity of a synthetic basalt during melting. *J. Geophys. Res.* **77**, 5665–5672 (1972).
22. Waff, H. S. & Bulau, J. R. Equilibrium fluid distribution in an ultramafic partial melt under hydrostatic conditions. *J. Geophys. Res.* **84**, 6109–6114 (1979).
23. Roberts, J. J. & Tyburczy, J. A. Partial-melt electrical conductivity: Influence of melt composition. *J. Geophys. Res.* **104**, 7055–7066 (1999).

24. Takahashi, E. Melting of a dry peridotite KLB-1 up to 14 GPa: Implications on the origin of peridotitic upper mantle. *J. Geophys. Res.* **91**, 9367–9382 (1986).
25. Kushiro, I. *et al.* Melting of a peridotite nodule at high pressures and high water pressures. *J. Geophys. Res.* **73**, 6023–6029 (1968).
26. Wyllie, P. J. & Huang, W-I. Influence of mantle CO_2 in the generation of carbonatites and kimberlites. *Nature* **257**, 297–299 (1975).
27. Wang, W. & Takahashi, E. Subsolidus and melting experiments of K-doped peridotite KLB-1 to 27 GPa: Its geophysical and geochemical implications. *J. Geophys. Res.* **105**, 2855–2868 (2000).
28. Holtzman, B. K. *et al.* Melt segregation and strain partitioning: implications for seismic anisotropy and mantle flow. *Science* **301**, 1227–1230 (2003).
29. Baba, K., Chave, A. D., Evans, R. L., Hirth, G. & Mckie, R. L. Mantle dynamics beneath the East Pacific Rise at 17°S: Insights from the Mantle Electromagnetic and Tomography (MELT) experiment. *J. Geophys. Res.* **111**, B02101, doi:10.1029/2004JB003598 (2006).
30. Dunn, R. A. & Forsyth, D. W. Imaging the transition between the region of mantle melt generation and the crustal magma chamber with short-period Love wave propagation along the southern East Pacific Rise. *J. Geophys. Res.* **108**, B72352, doi:10.1029/2002JB002217 (2003).

Supplementary Information is linked to the online version of the paper at www.nature.com/nature.

Acknowledgements We thank K. Baba, K. Fujita, M. Ichiki, T. Koyama, E. Ito and D. Yamazaki for discussions, D. Kohlstedt for comments and suggestions that improved manuscripts, and C. Oka for technical assistance.

Author Information Reprints and permissions information is available at www.nature.com/reprints. The authors declare no competing financial interests. Correspondence and requests for materials should be addressed to T.Y. (tyoshino@misasa.okayama-u.ac.jp).